Gamow-Teller beta decay of ^{29}Na and comparison with shell-model predictions

P. Baumann,[a] Ph. Dessagne,[a] A. Huck,[a] G. Klotz,[a] A. Knipper,[a] G. Marguier,[b] C. Miehé,[a] M. Ramdane,[a] C. Richard-Serre,[c] G. Walter,[a] and B. H. Wildenthal[d]

[a]*Centre de Recherches Nucléaires, 67037 Strasbourg, France and the Isolde Collaboration, CERN, 1211 Geneva 23, Switzerland*

[b]*Institut de Physique Nucléaire, 69622 Villeurbanne, France and the Isolde Collaboration, CERN, 1211 Geneva 23, Switzerland*

[c]*IN2P3 and the Isolde Collaboration, CERN, 1211 Geneva 23, Switzerland*

[d]*Department of Physics and Atmospheric Science, Drexel University, Philadelphia, Pennsylvania 19104*

(Received 23 March 1987)

Gamma radiation and delayed neutrons following the decay of 44.9 ms ^{29}Na have been studied in singles and coincidence mode with mass-separated sources. Evidence for a first excited state in ^{29}Mg at 54.6 keV has been found, in good agreement with theoretical predictions. From the lifetime, $\tau=1.83\pm0.10$ ns, deduced from γ-γ delayed coincidences with BaF_2 counters, a transition strength $B(M1)=0.11$ Weisskopf units is found for the 55 keV $(\frac{1}{2}^+)\rightarrow$g.s. $(\frac{3}{2}^+)$ transition. A level scheme built on the new state at 55 keV and involving five new transitions has been established for bound levels in ^{29}Mg. The features of these levels are compared with predictions of shell-model calculations, with which they substantially agree. In the neutron time-of-flight spectra, high-energy neutron branches have been found in addition to the previously reported decays. The observed distribution of the Gamow-Teller transition strengths with excitation energy for particle-unbound levels in ^{29}Mg is found to be shifted upward by about 1 MeV relative to shell-model predictions.

I. INTRODUCTION

As part of a study of the emission modes of ^{30}Na, we have been led to a new investigation of the level structure of ^{29}Mg. Several bound states of ^{29}Mg ($E_x<3.78$ MeV) are populated in the β decay of ^{30}Na through delayed one-neutron emission. Unbound states of ^{29}Mg ($E_x>3.78$ MeV) are involved in delayed two-neutron emission from ^{30}Na if this decay is a sequential process. Consequently, it is important to have a comprehensive description of the ^{29}Na beta decay to both bound and unbound states of ^{29}Mg. Furthermore, knowledge of Gamow-Teller (GT) decays with large Q values is in itself of fundamental interest, as it provides a measure of the intrinsic strength of this operator in nuclei and tests for shell-model calculations very far from stability. In *sd*-shell nuclei, the model space of the valence nucleons is relatively small and full-space shell-model calculations are possible. In the case of the neutron-rich Na and Mg nuclei, detailed predictions for the GT decay have been published.[2]

The decay modes of the heavy Na isotopes were studied extensively by Detraz *et al.*[3] and Guillemaud *et al.*[4] High-resolution energy spectra of delayed neutrons have been measured by Ziegert *et al.*[5] for $^{27-31}$Na. The level structure of the neutron-rich magnesium isotopes has been investigated with transfer reactions by Fifield *et al.*[6] In the case of the level scheme of ^{29}Mg, these authors propose a new interpretation of the experimental data of Ref. 4 which involves a level at 54 keV in ^{29}Mg. A low-energy doublet $(\frac{3}{2}^+, \frac{1}{2}^+)$ is predicted for this nucleus by shell model calculations[1,2,7–9] which employ an empirically renormalized effective Hamiltonian.

We have undertaken a study at the CERN on-line mass separator ISOLDE of the neutron and gamma emission modes which follow the beta decay of ^{29}Na and ^{30}Na. The aim of the study was to obtain a complete description of the β strength function to be compared to the *sd*-shell model predictions. In this paper, we report on the measurements of the ^{29}Na beta decay by neutron and gamma spectroscopy. In particular, we describe the experiments made to establish the existence of a level at low energy in ^{29}Mg and to measure its lifetime. The upper part of the beta strength function is deduced from the energy spectra of delayed neutrons obtained with the time-of-flight technique and from n-γ coincidence measurements. The data obtained are then compared with theoretical predictions.

II. EXPERIMENTAL PROCEDURE

The ^{29}Na isotope is produced by bombarding a uranium carbide target with a 2 μA proton beam of the 600 MeV CERN synchrocyclotron. The Na atoms are ionized by means of a tungsten surface-ionization source. The mass-separated ion beam is collected inside a thin cylindrical β detector on the Mylar tape of a transport system. The yield achieved at the ISOLDE facility for ^{29}Na was $\simeq 2.10^3$ atoms/sμA^{-1} in this experiment. The activity of this short-lived isotope [$T_{1/2}=44.9\pm1.2$ ms (Ref. 4)] is measured at the collection point. The descendants and contaminants are removed by driving the tape with a constant velocity of 30 cm/s. In order to detect low-energy gamma rays, we use an intrinsic germanium detector with a beryllium window placed in front of a

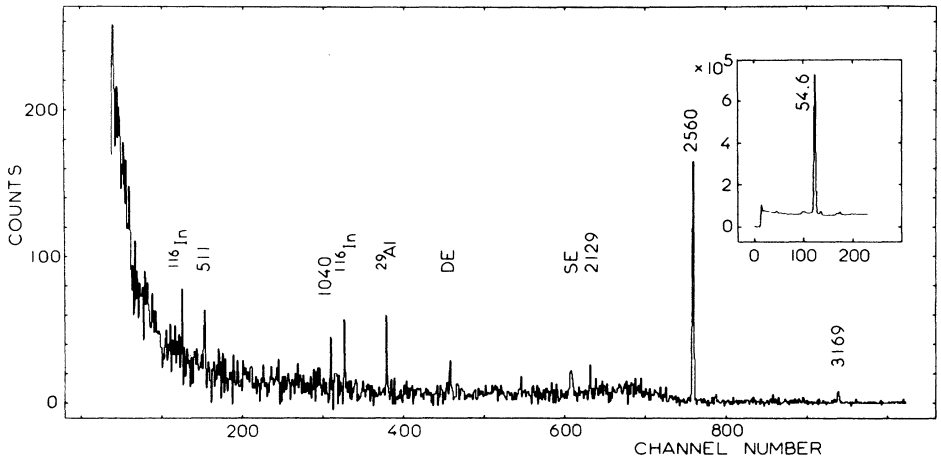

FIG. 1. Gamma-ray spectrum in coincidence with the 55 keV transition in ^{29}Mg (background has been subtracted). The peaks attributed to ^{29}Na decay are labeled with the corresponding γ-ray energy in keV. Descendant and contaminant activities are referred to the parent nucleus symbol (see text). The inset shows the low energy part of the direct γ spectrum registered with the intrinsic germanium detector.

thin ($\frac{1}{10}$ mm) aluminum wall to minimize the gamma absorption. A 33% Ge(Li) counter is placed at 90° with respect to the first one.

Beta-gamma and gamma-gamma coincidence measurements were made to elucidate the spectrum of ^{29}Mg. The lifetime associated with low-energy transitions was determined in a separate experiment which employed the delayed coincidence technique with two BaF_2 detectors. The fast component ($\tau \simeq 0.6$ ns) of the light emission from the BaF_2 crystal allows for very good timing[10,11] even at low energy. A small BaF^2 counter (diameter of 2 cm, length of 2 mm) optically coupled to a 56 DUVP photomultiplier tube detects low-energy gamma rays with an energy resolution of 42% at 60 keV. A large BaF_2 crystal (diameter of 10 cm, length of 14 cm) coupled to a EMI 9821QB photomultiplier tube is used for gamma rays in the 0.1–3.5 MeV energy range and yields an energy resolution of 11% at 662 keV and 7% at 2614 keV. This measurement requires a low-energy threshold ($\simeq 10$ keV) for the timing signals corresponding to the small counter. Triparametric γ-γ-t events are registered on magnetic tape for subsequent analysis.

For neutron energy measurements, the thin cylindrical β detector surrounding the collection point gives the start of the time of flight. Two large area (2880 cm^2) plastic scintillators were set up for neutron detection at a distance of 100 cm from the collection point. For isochronous flight paths, these scintillators are curved and centered at the collection spot. The thicknesses of the two neutron counters were different (1.25 and 5 cm), which implies a better resolution and a lower efficiency for the thinner one. A detailed description of the experimental arrangement is given elsewhere.[12] The two neutron counters were operated with a recoil proton detection threshold of 1.0 MeV. Two germanium counters were used in addition, to perform neutron-gamma coincidence measurements.

III. EXPERIMENTAL RESULTS

A. Gamma-ray spectra

The low-energy region of the direct gamma spectrum taken with the intrinsic germanium counter is presented in Fig. 1 (inset). We identify a gamma ray at 54.6±0.1 keV issuing from a strongly populated level. The gamma rays detected with the Ge(Li) counter in coincidence with the 55 keV line are also shown in Fig. 1. The coincidence measurements clearly indicate the existence of a level at 55 keV fed by several transitions: 1040, 2129, 2560, and 3169 keV. In Table I we list the energies, relative intensi-

TABLE I. Energies and relative intensities of gamma rays following β decay of ^{29}Na attributed to transitions between levels in ^{29}Mg. The relative intensity of the 55 keV gamma ray could not be measured with accuracy in our experimental conditions, in which the corrections for gamma absorption at low energy are strongly dependent on the position of the source on the moving tape.

E_γ (keV)	I_γ(relative) (%)	$E_i - E_f$ (keV)
54.6±0.1	≥115	55–0
1039.9±0.2	4.6±0.3	1095–55
1585.6±0.2	15.6±0.9	3224–1638
1638.0±0.2	16.3±0.9	1638–0
2129.0±0.6	3.7±0.3	3224–1095
2132.8±0.8	1.5±0.2	3227–1095
2445.1±1.3	0.4±0.1	2500–55
2499.9±1.3	0.2±0.1	2500–0
2560.2±0.4	100	2615–55
2614.8±0.5	4.7±0.3	2615–0
3169.0±0.8	10.3±0.6	3224–55
3172.6±1.0	0.4±0.1	3227–55
3223.6±1.0	4.4±0.4	3224–0
3227.3±1.0	6.6±0.5	3227–0
3673.9±1.5	2.3±0.2	3674–0
3985.4±1.5	0.8±0.1	3985–0

TABLE II. Gamma-ray branching ratios in ^{29}Mg.

E_i (keV)	E_f (keV)	This work
55	0	100
1095	55	100
1638	0	100
2500	0	38±6
	55	62±6
2615	0	4.5±0.3
	55	95.5±0.3
3224	0	13±1
	55	30±2
	1095	11±1
	1638	46±2
3227	0	78±2
	55	5±1
	1095	17±2
3674	0	100
3985	0	100

ties, and assignments of gamma rays following the beta decay of ^{29}Na. Experimental branching ratios of the levels which give rise to these gamma rays are listed in Table II.

In the gamma spectra, we observe, in addition to these ^{29}Mg transitions, lines corresponding to the decay of contaminant nuclei ^{116}Ag and ^{116}In. These atoms ($4^+, A=116$) are not separated from the singly charged $A=29$ beam because they have the same energy-to-charge and mass-to-charge ratios.

The intensities of the β branches are deduced from the imbalances of the γ intensities feeding and emitting from the various levels. As we have no precise value for the relative intensity of the 55 keV transition, we indicate for the total β feeding of the ground and 55 keV state the value given in Ref. 4 for the unobserved β transitions.

The logft values listed in Table III for β branches to bound levels in ^{29}Mg are deduced from our results by making use of values given in Refs. 4 and 13 for $T_{1/2}$, Q_β, and P_n. Among the lines attributed to the ^{29}Na decay are four which correspond to transitions between levels of ^{28}Mg (Table IV). These allow us to determine the intensities of neutron branches to four excited states in the residual nucleus ^{28}Mg (1.47, 3.86, 4.55, and 4.56 MeV).

B. Lifetime measurement of the 55 keV level in ^{29}Mg

The 2560 and 3169 keV gamma rays, which are the main branches to the 55 keV level, are well separated in energy (Fig. 2), so that energy selection can be done with the BaF_2 detectors. We have analyzed the time spectra corresponding to the windows on the full-energy peaks of the 2.56→0.055 and 3.17→0.055 MeV cascades. The resulting delayed curve in the first case is shown in Fig. 3 (curve A). The prompt curve (B) [full width at half maximum (FWHM) of 1.4 ns] is obtained with gates placed on the 1.29 MeV gamma ray (^{116}In) and in the 100 keV region of the spectrum (inset of Fig. 2). The calibration of the time axis has been obtained by registering the prompt curve with different calibrated delays. From a least-squares fit on the data we have deduced the value of 409±0.88 ps/channel. The analysis has been done on the delayed component of the coincidence curves. A weighted least squares fit on the experimental decay curve leads to the value of $\tau=1.84\pm0.12$ ns, in very good agreement with the value deduced from the other weaker cascade ($\tau=1.79\pm0.18$ ns). For these values, the statistical error is dominant and the time-calibration error can be neglected. From these considerations we adopt for the lifetime

TABLE III. β branching, logft, and B(GT) values observed for bound levels (^{29}Mg) in the ^{29}Na decay together with predicted B(GT) values. As we have no precise value for the relative intensity of the 55 keV transition, we indicate, for the total β feeding of the ground and the 55 keV excited states, the value given in Ref. 4 for the unobserved β transitions.

E_x (keV)	I_β (%)	logft	B(GT)$_{expt}$	B(GT)$_{theor}$ (free nucleon)
0				0.0115
	24±10	5.3±0.2	0.031	
55				0.111
1095	<0.2	>7.0	<0.0006	
1638	<0.4	>6.6	<0.0015	0.003
2500	0.22±0.05	6.7±0.1	0.0012	0.005
2615	37.8±7.2	4.4±0.1	0.245	0.373
3224	12.3±2.4	4.8±0.1	0.097	0.261
3227	3.1±0.6	5.4±0.1	0.0245	0.074
3674	0.8±0.2	5.9±0.1	0.007	0.035
3985	0.29±0.06	6.2±0.1	0.004	0.032
			$\sum$ =0.410	=0.906

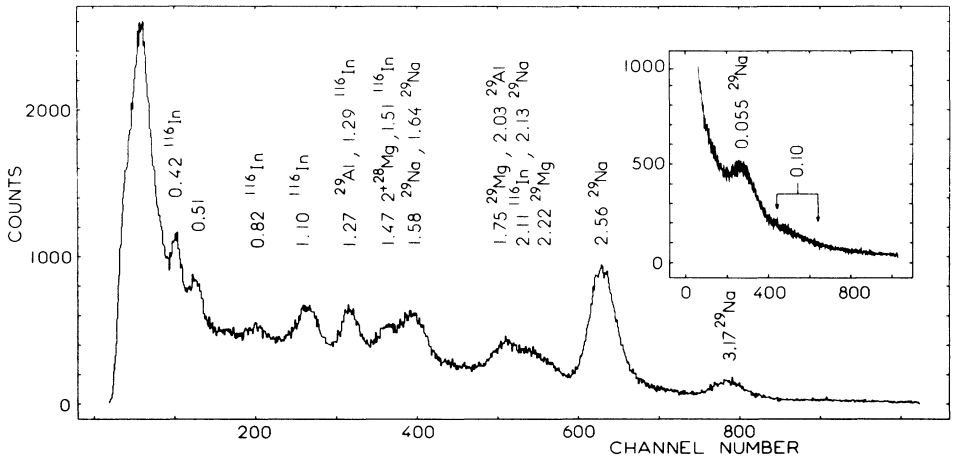

FIG. 2. Gamma-ray spectrum following ^{29}Na β decay and recorded with the large BaF_2 detector in coincidence with the small BaF_2 (lines at 2.56 and 3.17 MeV which have been used to gate the 55 keV lifetime measurement are indicated). In the inset the low energy part of the corresponding spectrum, registered with the small detector, is represented.

of the 55 keV level the weighted mean value of $\tau = 1.83 \pm 0.10$ ns, the quoted error being slightly overestimated.

C. Delayed neutron spectra

As the low-energy spectrum ($E_n < 2$ MeV) of the delayed neutrons has been extensively studied by Ziegert *et al.*,[5] the aim of our measurements with the time-of-flight technique was to obtain evidence on possible neutron emission at higher energy and also information from n-γ coincidences. The neutron spectrum measured with the curved scintillator (thickness of 1.25 cm) is presented in Fig. 4. In addition to the two peaks ($E_n = 1.70 \pm 0.01$ and 2.25 ± 0.01 MeV), which can be related to lines observed at 1.702 and 2.250 MeV in the high resolution work,[5] this measurement reveals strong high-energy peaks. This spectrum was analyzed by taking into account the energy resolution of the detector and its variation over the range of detected events. In this analysis, it was not possible to fit the neutron distribution with one or even several line shapes in three regions of energy, and only limits have been indicated for the emitted neutron energies. The relative intensities of the different components are reported in Table V after corrections for efficiency and a detection threshold at 1 MeV. The relative efficiency decreases from 9.8% to 8.5% as the neutron energy rises from 1.7 to 6 MeV.

The different neutron groups listed in Table V are assumed to be transitions to the ground state of ^{28}Mg unless indications are found in the gamma-neutron coincidence measurements for population of the 2^+ state in the final nucleus. Coincident events have only been observed in the case of the neutron group at 2.57 MeV.

We make use of the various available results in order to

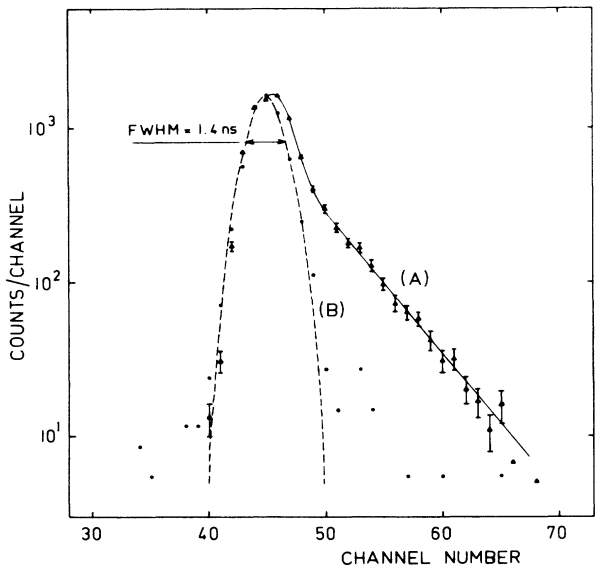

FIG. 3. Delayed coincidences (curve *A*) taken in the decay of ^{29}Na with two BaF_2 detectors recording the 2.56→0.055 MeV cascade. The experimental prompt curve (curve *B*) is fitted by a Gaussian function (dashed line) with a FWHM of 1.4 ns.

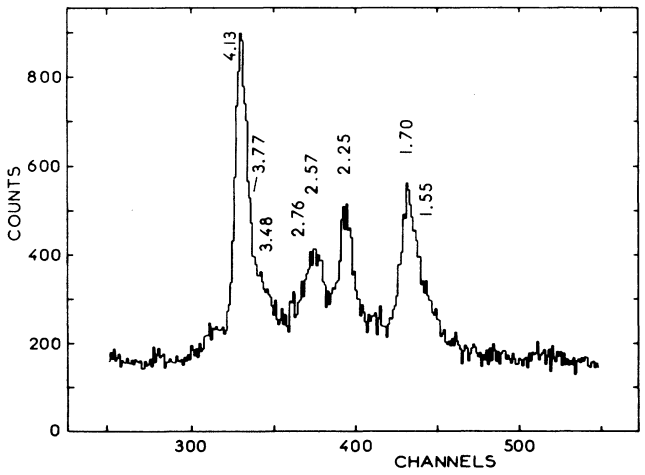

FIG. 4. Neutron time-of-flight spectrum related to the ^{29}Na decay.

TABLE IV. Energies and relative intensities of gamma rays following β decay of ^{29}Na and attributed to transitions between levels in ^{28}Mg. Intensities are normalized to the main gamma line (2560.2 keV) registered in the ^{29}Na decay.

E_γ (keV)	I_γ(relative) (%)	$E_i - E_f$ (keV)
1474.0±0.2	18.4±1.0	1474 − 0
2389.8±0.5	0.6±0.1	3863 − 1474
3080.9±1.0	0.17±0.05	4555 − 1474
3084.8±1.0	0.15±0.04	4559 − 1474

establish the decay scheme to particle-unbound excited states in ^{29}Mg. The low-energy part of the neutron spectrum is taken from Ziegert *et al.*,[5] while at higher energies results are inferred from this experiment. The two measurements can be normalized through the intensity of the 1.7 MeV neutron peak, which is recorded in both experiments. The β feeding to the neutron-emitting states is obtained by normalizing the total intensity of the neutron lines to the known one-neutron emission probability (P_{1n}21.5%, Ref. 3).

From the comparison of the neutron spectra normalized to the 1.7 MeV peak, it appears that 50.6% of the neutron emission is observed for $E_n > 1.7$ MeV in the time-of-flight experiment, whereas 49.4% of the emission corresponds to neutrons with $E_n \leq 1.7$ MeV, detected with high-resolution techniques.[5] In the analysis of Ref. 5, the five strongest neutron peaks were assumed to represent ground-state transitions and all weaker lines were assumed to correspond to transitions to the first excited state in ^{28}Mg. With our results, this interpretation cannot give an account of the 6.6% β feeding of the 2^+ state measured in our gamma experiment since only one neutron branch ($E_n = 2.57$ MeV) has been observed to populate this level in the high-energy neutron spectrum. At least one strong peak of the low-energy neutron spectrum should be included in the branches populating the 2^+ state and we suggest it should be the 512 keV neutron peak on the following grounds:

(i) The branching ratios to the 0^+ and 2^+ states obtained in this way are comparable to the experimental values.

TABLE V. Energies and relative intensities of neutrons following β decay of ^{29}Na and corresponding excitation energies in ^{29}Mg.

E_n (MeV)	I_n(relative) (%)	E_x(^{29}Mg) (MeV)
1.70±0.01	100	5.54±0.03
[1.84 − 2.07]	31.7±5.5	[5.69 − 5.92]
2.25±0.01	92.1±16.0	6.11±0.03
2.57±0.02	38.8±6.7	7.92±0.04
2.76±0.02	39.2±6.8	6.64±0.04
[2.92 − 3.30]	29.1±5.0	[6.81 − 7.20]
3.48±0.04	23.2±4.0	7.39±0.05
3.77±0.04	33.9±5.9	7.69±0.05
4.13±0.02	115.5±20	8.05±0.04
[4.54±5.58]	20.7±3.6	[8.48 − 9.56]

(ii) The excitation energy of the level emitting the 512 keV neutron ($E_x = 5785$ keV) is, in this case, consistent with the value corresponding to the emission of 1930 keV neutrons, observed in both experiments ($E_x = 5780$ keV).

It should be noted that the intensities of the branches to the levels at 3.86, 4.55, and 4.56 MeV, for which the gamma decay has been measured, are too weak to be related to the observed neutron branches and far too weak to appear in the neutron-gamma measurements.

In Table VI we report β branching, logft, and B(GT) values for unbound levels of ^{29}Mg in the ^{29}Na decay. At low energies, the values for neutrons are taken from Ref. 5 and intensities are normalized as described before. The logft and B(GT) calculations have been made using the same values for $T_{1/2}$, Q_β, and P_n as in the preceding section.

IV. DISCUSSION

A. Shell-model predictions

We compare the experimental features of ^{29}Mg determined in the present and past[3–6] work with predictions of the "USD" (unified *sd*) effective Hamiltonian.[2,9] The USD two-body matrix elements and single-particle energies were determined by requiring a least-squares fit between 440 experimental level energies of $A = 18$–38 nuclei and the corresponding shell-model eigenvalues generated in complete $d_{5/2}$-$s_{1/2}$-$d_{3/2}$ configuration spaces. In this fitting procedure, the two-body matrix elements were scaled by a factor of $A^{-0.3}$. With this mass dependence it was possible to obtain eigenvalues from a single Hamiltonian formulation that agreed with experiment across the entire $A = 18$–38 region.

Earlier attempts to obtain empirically optimum effective Hamiltonians for *sd*-shell nuclei[7,8] assumed two-body matrix elements which were constant, independent of A. These Hamiltonians could reproduce experimental energies only over limited ranges of *sd*-shell nuclei. The first predictions[1] for the energy-level structure of ^{29}Mg were generated from the Preedom-Wildenthal interaction.[7] In the salient feature of predicting a ground-state $\frac{3}{2}^+$-$\frac{1}{2}^+$ doublet, the Preedom-Wildenthal results are similar to those obtained with the present USD interaction.

Wave functions for states of ^{29}Na and ^{29}Mg were generated for the present study by diagonalizing the USD Hamiltonian in the complete *sd*-shell configuration space for the appropriate combinations of J and T. For the states of $\frac{1}{2}^+$, $\frac{3}{2}^+$, and $\frac{5}{2}^+$ in ^{29}Mg, the diagonalizations were extended in excitation energies up to the maximum value allowed by the Q value for beta decay from ^{29}Na. These wave functions and their eigenvalues were then used in the calculation of $E2$, $M1$, and Gamow-Teller matrix elements. In such calculations, the transition operators can be assigned the "free-nucleon" coupling constants, taken from the properties of the free neutron and proton, or, alternatively, effective coupling constants which compensate for the omission of shell-model configurations other than those of the *sd* shell and for the neglect of mesonic and subnuclear degrees of freedom.

TABLE VI. β branching, logft, and B(GT) values of the unbound, levels of ^{29}Mg inferred from the measured spectrum of delayed neutron emission from ^{29}Mg. For those branches marked with an asterisk, a neutron transition to the 2^+ state of ^{28}Mg is assumed, whereas excitation energies are deduced on the assumption of ground state population in the final nucleus for other branches (see text).

E_n (keV)	$E_x(^{29}\text{Mg})$ (keV)	I_β (%)	logft	$B(\text{GT})_{\text{expt}}$
110*	5369	0.3±0.05	5.9±0.02	0.007
185	3972	1.45±0.23	5.5±0.1	0.0195
339	4132	1.27±0.2	5.6±0.1	0.0155
376*	5644	0.72±0.12	5.4±0.1	0.0245
512*	5785	1.37±0.22	5.1±0.1	0.049
808*	6092	0.27±0.04	5.7±0.1	0.0123
1050*	6342	0.42±0.07	5.5±0.1	0.0195
1103*	6397	0.32±0.05	5.6±0.1	0.0155
1190*	6487	0.19±0.03	5.8±0.1	0.010
1371*	6675	0.22±0.04	5.7±0.1	0.0123
1555	5391	0.70±0.11	5.5±0.1	0.0195
1702	5544	2.63±0.42	4.9±0.1	0.078
[1840−2070]	[5690−5920]	0.84±0.17	[5.2−5.4]	0.031
2250±10	6110±30	2.42±0.50	4.8±0.1	0.097
2570±20*	7920±40	1.02±0.20	4.6±0.1	0.155
2760±20	6640±40	0.79±0.16	5.1±0.1	0.049
[2920−3300]	[6810−7200]	0.76±0.15	[4.9−5.1]	0.062
3480±40	7385±50	0.61±0.12	5.0±0.1	0.062
3770±40	7685±50	0.89±0.18	4.7±0.1	0.123
4130±20	8058±40	3.04±0.61	$4.1^{+0.3}_{-0.08}$	0.490
[4540−5580]	[8480−9560]	0.54±0.11	[4.2−4.6]	0.245

For $E2$ matrix elements, it is conventional to assume added charges for the neutron and proton in order to generate model magnitudes as large as those experimentally observed. In this work the assumed harmonic oscillator radial wave functions and added charges of $0.35e$ for both the neutron and proton, choices consistent with other applications[9] of the USD wave functions. The free-nucleon form of the $M1$ operator in combination with the USD wave functions provides theoretical values of $M1$ matrix elements which are comparable in magnitude to experimental values on average. However, better case-by-case agreement between theory and experiment can be obtained with an effective $M1$ operator.[16] Finally, the free-nucleon form of the Gamow-Teller operator in combination with the USD wave functions yields theoretical transition strengths which are consistently larger than experimental values. An effective GT coupling constant equal to 0.76 times the free-nucleon value produces agreement between the experimental magnitudes of GT matrix elements observed for typical low-Q-value GT beta decays and the USD predictions.[17]

For the present study we calculate the branching ratios for the electromagnetic decays of the low-lying levels of ^{29}Mg by using the theoretical decay energies, the $E2$ operator described above, and the free-nucleon $M1$ operator. For the transition between the states of the $\frac{1}{2}^+$ and $\frac{3}{2}^+$ ground-state doublet, we present results obtained with both the free-nucleon and the effective $M1$ operators. Since the effective GT operator differs little from a simple quenching of the free-nucleon operator, the predicted Gamow-Teller strengths for the beta decay from ^{29}Na to ^{29}Mg are calculated only with the free-nucleon operator. The effective values are then obtained simply by scaling the free-nucleon values by $(0.76)^2$.

B. Spin-parity assignments and electromagnetic decay of particle-bound levels

The nuclei ^{29}Mg and ^{29}Na each have spin-parity values $J^\pi=\frac{3}{2}^+$ for their ground states.[4] The assumption of an allowed beta decay from ^{29}Na to the 55 keV level of ^{29}Mg thus implies that it has a positive parity and a range of spins $J=\frac{1}{2}-\frac{5}{2}$. Multipolarities of the gamma radiation deexcitating the 55 keV level higher than dipole are excluded by the lifetime determination, thus eliminating $J=\frac{5}{2}$. As noted above, shell-model calculations as well as simple consideration of single-particle energy orderings suggest that the lowest two states in ^{29}Mg should have J^π values of $\frac{3}{2}^+$ and $\frac{1}{2}^+$. We assume in the remaining dis-

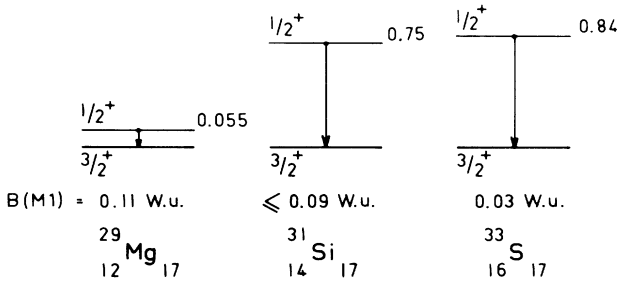

FIG. 5. Systematics of $M1$ ($\frac{1}{2}^+\rightarrow\frac{3}{2}^+$) transitions in $N=17$ isotones ($A=29$ from this work and $A=31,33$ from Ref. 14).

TABLE VII. Measured and calculated values of the $M1$ matrix element between the lowest $\frac{1}{2}^+$ and $\frac{3}{2}^+$ states in $N=17$ odd-mass nuclei.

	$\sqrt{(2J_i+1)B(M1)}\ \mu_N$		
Z	Expt.	Theor. (free nucleon)	Theor. (effective)
12 (Mg)	0.62±0.02	0.49	0.58
14 (Si)	≤0.59±0.06	0.43	0.52
16 (S)	0.333±0.004	0.25	0.34

cussion that the 55 keV level has $J^\pi=\frac{1}{2}^+$.

The lifetime we determine for the decay of the 55 keV level yields a $B(M1)$ value of 0.11±0.01 W.u. under the (reasonable) assumption of a pure $M1$ decay, or, equivalently, an $M1$ matrix element of 0.62±0.02 μ_N. This value is quite consistent with the known trends of similar $M1$ decays. These trends are summarized in Fig. 5, which shows the excitation energies and $B(M1)$ values between $\frac{1}{2}^+$ first excited states and $\frac{3}{2}^+$ ground states for the $N=17$ systems ^{29}Mg, ^{31}Si, and ^{33}S, and in Table VII, which lists the experimental values of these $M1$ matrix elements and the corresponding shell-model predictions based both on the free-nucleon and the effective forms of the $M1$ operator.

We see from Table VII that the observed trend of the matrix element values is reproduced with both operators and that the absolute values obtained with the effective operator are very close to the measured values for all three systems. It might be noted that the simplest characterization of the effective $M1$ operator is that it represents a quenching of the free-nucleon value, just as in case of the Gamow-Teller operator. The $M1$ case is not so simple as the Gamow-Teller case, however, as is evident from Table VII. The effective operator enhances, rather than quenches, the values of the $\frac{1}{2}^+$-$\frac{3}{2}^+$ transitions.

Our knowledge about the higher-lying particle-bound states in ^{29}Mg is limited to their excitation energies, their population by beta decay from ^{29}Na, and the branching ratios of their electromagnetic decay. The level scheme of bound levels of ^{29}Mg established from our measurements is shown in Fig. 6 along with the corresponding predictions of the USD calculations. Of the ten model levels predicted to occur below 4 MeV excitation energy, only one, the $\frac{7}{2}^+$ at 2106 keV, would not be populated by an allowed beta transition from ^{29}Na. The others all have J^π values of $\frac{1}{2}^+$, $\frac{3}{2}^+$, or $\frac{5}{2}^+$. No additional model levels of these three spins are predicted below 4.8 MeV. Our data indicate ten levels in the experimental spectrum of ^{29}Mg below 4 MeV excitation energy.

The observed and calculated gamma-ray branching ratios for these levels are indicated in Fig. 6. From a consideration of the energies and the branching ratios, along with the measured and calculated beta decay strengths, it seems plausible to associate the observed level at 1638 keV with the first $\frac{5}{2}^+$ model state predicted to occur at 1542 keV. The gamma decay of both states is dominated by the (largely $M1$) decay to the lowest $\frac{3}{2}^+$ state. The previously unobserved experimental level at 2500 keV, with its 4:6 ratio of decay intensity to, respectively, the $\frac{3}{2}^+$ and $\frac{1}{2}^+$ members of the ground state doublet, appears to correspond to the second model level with $J^\pi=\frac{3}{2}^+$ which occurs at 2193 keV excitation energy and decays with a 3:7 ratio to these same two states. We note that a level at 2.48 MeV excitation energy in ^{29}Mg was reported from the study of heavy-ion transfer reaction experiments.[6]

The experimental level at 2615 keV is strongly fed in beta decay. This and its measured 4:96 branching ratio to the $\frac{3}{2}^+$, $\frac{1}{2}^+$ doublet strongly argue for the association of this level with the second model $\frac{1}{2}^+$ state, which occurs at 2438 keV excitation energy, has a dominant feeding in

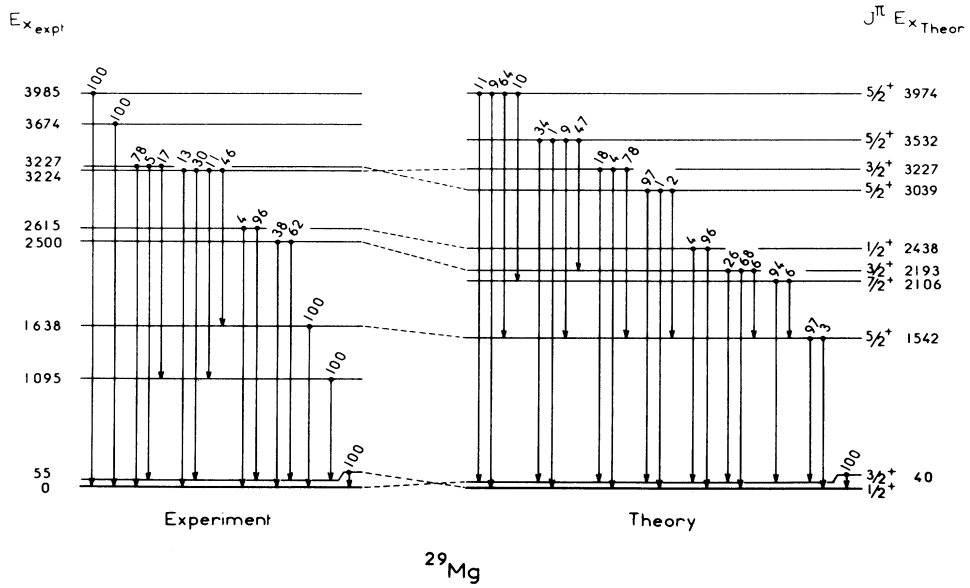

FIG. 6. Comparison of observed and calculated properties of levels in ^{29}Mg.

beta decay and has a predicted 4:96 branching ratio for the gamma decay to the $\frac{3}{2}^+, \frac{1}{2}^+$ doublet. A doublet of levels, at 3224 and 3227 keV, is found next in the experimental spectrum of ^{29}Mg. The 3224 keV member is characterized by a large matrix element for beta decay from ^{29}Na, an inhibited gamma decay to the lowest $\frac{3}{2}^+$ state, and a dominant gamma decay to the lowest $\frac{5}{2}^+$ state. These properties correspond closely to those of the third model $\frac{3}{2}^+$ state, which occurs at 3227 keV in the model spectrum. The experimental level at 3227 keV is characterized by a dominant gamma decay to the lowest $\frac{3}{2}^+$ state. On this basis and its energy we associate it with the second model $\frac{5}{2}^+$ level, which is found at 3039 keV excitation energy.

Experimental levels are assigned to excitation energies of 3674 and 3985 keV on the basis of gamma ray lines of the same energies. These two states correspond closely in energy to the third and fourth model $\frac{5}{2}^+$ states, which are predicted to occur at 3532 and 3974 keV excitation energy. However, the predicted gamma decays of these model states are not strongly dominated by branches to the lowest $\frac{3}{2}^+$ state or, indeed, to any single state. Hence, while the two observed states between 3.5 and 4.0 MeV excitation energy are a nice match for the model predictions of only two otherwise unaccounted for states in this energy range, there are significant discrepancies between the observed and predicted decay patterns.

The final element to consider in the observed level scheme of the bound states of ^{29}Mg is the 1095 keV level. There is no logical match for this level in the model spectrum of states from the *sd*-shell configuration space. In accord with the analysis of Ref. 6, we would assume that this state has negative parity and a probable spin of $\frac{3}{2}$. This assumption is consistent with our experimental results, in which no beta feeding for this state has been found in the decay of ^{29}Na, while at the same time it is strongly populated by one-neutron decay from ^{30}Na.

C. Particle-unbound levels of ^{29}Mg and the total spectrum of Gamow-Teller strength from ^{29}Na

The dominant features of the measured spectrum of delayed-emission neutrons are several strong groups corresponding to the deexcitation of high-lying levels of ^{29}Mg. The Gamow-Teller strength which is associated with the population of these levels from ^{29}Na is a significant fraction of the total strength of the ^{29}Na decay. Our experimental results indicate that 51% of the emitted neutrons have energies higher than 1.7 MeV. In spite of the difficulties in assigning initial and final levels in delayed neutron emission, it appears clear that the neutron decay is concentrated in a limited number of particle-unbound excited states in the region of excitation energy which extends up to 9 MeV in ^{29}Mg.

The experimental values of B(GT) extracted from our measurements for the particle-bound states of ^{29}Mg are listed in Table III, together with the shell-model predictions based on the free-nucleon Gamow-Teller operator. The experimental values of B(GT) for the particle-unbound states are listed in Table VI. The composite experimental and shell-model spectra for all states in the excitation energy range 0–9.6 MeV are plotted in Fig. 7 in both differential (top panels) and integral (bottom panels) representations. The differential plots of B(GT) versus excitation energy (strength is summed in 200 keV bins) show two dominant peaks in the bound-state region, at 2.5 and 3.3 MeV excitation energy, in both the experimental and the shell-model plots. In the particle-unbound (delayed neutron) region, the experimental spectrum of strength is characterized by a plateau of strength from 5 to 8 MeV excitation energy followed by a dominant peak of strength at 8.05 MeV excitation energy, corresponding to the 4.13 MeV neutron group. The shell-model spectrum shows a cluster of strength around 5 MeV excitation energy and a dominant peak at about 7.2 MeV excitation energy. The integral plots reflect these same features, of course, but emphasize the overall trends

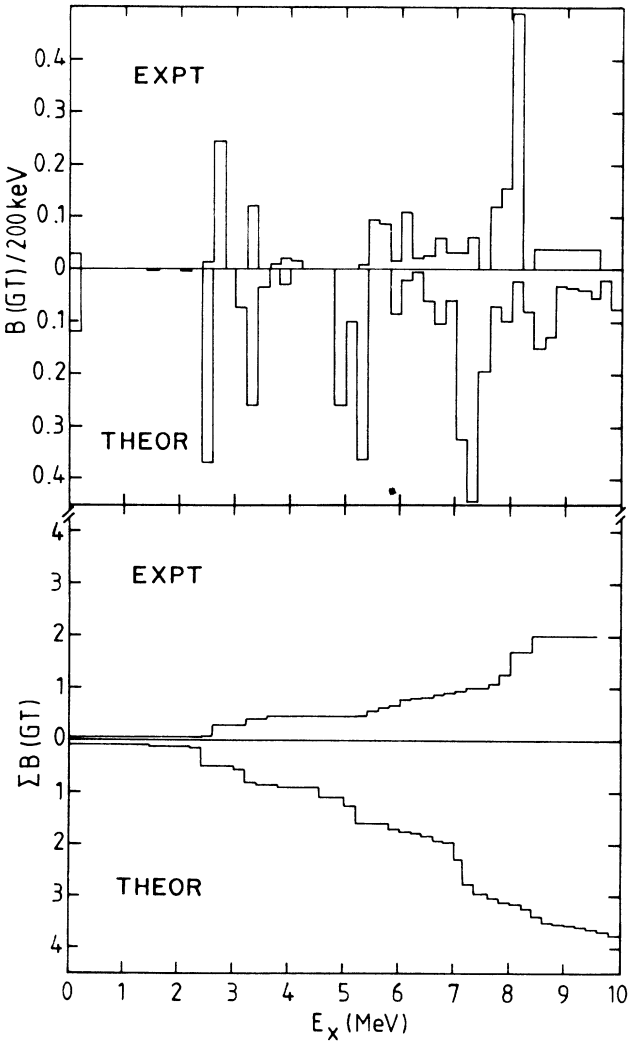

FIG. 7. B(GT) strength distribution for the beta decay of ^{29}Na. In the upper two panels experimental and theoretical strength within each 200 keV energy bite is summed and these values are plotted as histograms. In the lower two panels the integral of the GT strengths are plotted.

of strength versus energy.

The essential differences between the measured and the predicted distributions of Gamow-Teller strength are the displacement, relative to experiment, of theoretical strength in the particle-unbound region to lower (about 1 MeV) excitation energies and the overall smaller magnitudes of observed strength relative to the shell-model predictions. The difference in the overall normalization of shell-model versus experimental Gamow-Teller strength is completely consistent with existing knowledge about *sd*-shell nuclear structure.[15–17] The ratio of observed Gamow-Teller strength to that predicted from the USD wave functions with the free-nucleon normalization is 0.45 for the states in the particle-bound region and 0.5 for the entire 9.6 MeV span of measurement and calculation. These quenching factors of experiment relative to theory are to be compared with the global average quenching factor for the low-lying beta decay in the *sd* shell of 0.56.[17] In the context of the uncertainties attendant to the present experimental normalization, the present quenching factor is consistent with this "standard" value.

It is worth noting that the Gamow-Teller strength from ^{29}Na that is located below 9.6 MeV excitation energy in ^{29}Mg amounts to only about $\frac{1}{10}$ of the total decay strength from this parent state. Hence, the extracted ratio of experiment to theory depends sensitively upon the detailed energy distributions of this strength. The dislocation in excitation energies of the strength concentrations in the 4.0–9.6 MeV region between the model predictions and the experimental results should be considered in this light. Such discrepancies between experiment and theory are not outside the range of findings for nuclei closer to stability and perhaps represent no more than the intrinsic noise of the present level of model accuracy. On the other hand, the proximity of the presently studied systems to the onset of strong deformations which invert the normal ordering of the shell-model orbits, a symptom of which is provided by the 1095 keV state, may underly this discrepancy in the distribution of Gamow-Teller strength.

Further detailed study of the structure of neutron-rich nuclei near $N=20$ should help clarify these questions.

ACKNOWLEDGMENTS

The authors are indebted to the Crystal Castle Collaboration of Strasbourg for the loan of the barium fluoride detectors and wish to thank P. Engelstein for helpful discussions concerning time measurements. The research was supported in part (B.H.W.) by the U.S. National Science Foundation under Grant No. PHY-85-09736.

[1]B. J. Cole, A. Watt, and R. R. Whitehead, J. Phys. A **7**, 1399 (1974).

[2]B. H. Wildenthal, M. S. Curtin, and B. A. Brown, Phys. Rev. C **28**, 1343 (1983).

[3]C. Detraz, D. Guillemaud, G. Huber, R. Klapisch, M. Langevin, F. Naulin, C. Thibault, L. C. Carraz, and F. Touchard, Phys. Rev. C **19**, 164 (1979).

[4]D. Guillemaud-Mueller, C. Detraz, M. Langevin, F. Naulin, M. de Saint-Simon, C. Thibault, F. Touchard, and M. Epherre, Nucl. Phys. **A426**, 37 (1984); D. Guillemaud, Ph.D. thesis, Université Orsay, 1982 (unpublished).

[5]W. Ziegert, L. C. Carraz, P. G. Hansen, B. Jonson, K. L. Kratz, G. Nyman, H. Ohm, H. L. Ravn, and A. Schröder, in Proceedings of the 4th International Conference on Nuclei Far From Stability, Helsingor, 1981, CERN Report 81-09, 1981, p. 327.

[6]L. K. Fifield, P. V. Drumm, M. A. C. Hotchkis, T. R. Ophel, and C. L. Woods, Nucl. Phys. **A437**, 141 (1985).

[7]B. M. Preedom and B. H. Wildenthal, Phys. Rev. C **6**, 1633 (1972).

[8]W. Chung, Ph.D. thesis, Michigan State University, 1976 (unpublished).

[9]B. H. Wildenthal, Prog. Part. Nucl. Phys. **11**, 5 (1983).

[10]M. Laval, M. Moszynski, R. Allemand, E. Cormoreche, P. Guinet, R. Odru, and J. Vacher, Nucl. Instrum. Methods **206**, 169 (1983).

[11]F. A. Beck, *Properties of Large BaF_2 Crystals. Application as Fast and Efficient Gamma-Ray Detectors in the 4π-Crystal Castle Array*, Vol. 7 of *Nuclear Science Research Conference Series*, Oak Ridge, 1984 (Hardwood, New York, 1984).

[12]A. Huck, G. Klotz, A. Knipper, C. Miehé, C. Richard-Serre, G. Walter, A. Povès, H. L. Ravn, and G. Marguier, Phys. Rev. C **31**, 2226 (1985).

[13]T. Björnstad, H. A. Gustafsson, P. G. Hansen, B. Jonson, V. Lindfors, S. Mattsson, A. M. Poskanzer, and H. L. Ravn, Nucl. Phys. **A359**, 1 (1981).

[14]P. M. Endt, At. Data Nucl. Data Tables **23**, 3 (1979); P. M. Endt and C. van der Leun, Nucl. Phys. **A310**, 1 (1978).

[15]T. Björnstad, M. J. G. Borge, P. Dessagne, R. D. von Dinklage, G. T. Ewan, P. G. Hansen, A. Huck, B. Jonson, G. Klotz, A. Knipper, P. O. Larsson, G. Nyman, H. L. Ravn, C. Richard-Serre, K. Riisager, D. Schardt, and G. Walter, Nucl. Phys. **A433**, 283 (1985).

[16]B. A. Brown and B. H. Wildenthal, Phys. Rev. C **28**, 2397 (1983).

[17]B. A. Brown and B. H. Wildenthal, At. Data Nucl. Data Tables **33**, 347 (1985).